RSC Advances

RSC Advances

www.rsc.org/advances

www.rsc.org/advances

Melamine $\xrightarrow[\text{500 °C 4 h}]{\text{calcination}}$ Nanoplates g-C_3N_4

Melamine $\xrightarrow[\text{200 °C 12 h}]{\text{hydrothermal}}$ $\xrightarrow[\text{500 °C 4 h}]{\text{calcination}}$

Melamine $\xrightarrow[\text{200 °C 24 h}]{\text{hydrothermal}}$ $\xrightarrow[\text{500 °C 4 h}]{\text{calcination}}$ Nanotube g-C_3N_4

Journal Name

COMMUNICATION

Synthesis high specific surface area nanotube g-C$_3$N$_4$ with two-step condensation treatment of melamine to enhance photocatalysis properties

Zhengyuan Jin[a], Qitao Zhang[a], Saisai Yuan[a], Teruhisa Ohno[a, b, c, d] *

High specific surface area nanotube g-C$_3$N$_4$ was fabricated by a simple two-step condensation method. Photocatalytic activity was evaluated by decomposition of Rhodamine B (Rh B) under visible light. Nanotube g-C$_3$N$_4$ showed 12 times higher photocatalytic activity than that of bulk g-C$_3$N$_4$. The improvement of photocatalytic activity was mainly due to the higher surface area, the unique morphology and the number of defects.

Introduction

Photocatalysts have been studied for many years since the report by Fujishima and Honda showing that TiO$_2$ can be used to catalytically decompose H$_2$O to produce hydrogen under light irradiation.[1] Meanwhile, graphitic carbon nitride (g-C$_3$N$_4$), which is an organic semiconductor with visible-light absorption, high reduction ability and high chemical stability,[2] has recently received much attention as a metal free photocatalyst. Although the rates of degradation of harmful organic materials by g-C$_3$N$_4$ were generally smaller than those by TiO$_2$-based photocatalysts under UV light, g-C$_3$N$_4$ has a great advantage in that it works under visible light, absorbing blue light along with UV light.

In past years, g-C$_3$N$_4$ was widely used in composite photocatalysts such as g-C$_3$N$_4$/WO$_3$, g-C$_3$N$_4$/sulfur-doped TiO$_2$ and g-C$_3$N$_4$/TaON.[3-5] Although the activities of composite photocatalysts have been enhanced, the results have not been as good as expected. This is because original g-C$_3$N$_4$, which was obtained by high temperature condensation of melamine, dicyandiamide or cyandiamide, has suffered from the problem of having a low specific surface area. The specific surface area of original g-C$_3$N$_4$, which is normally below 10

a Department of Material Science, Faculty of Engineering, Kyushu Institute of Technology, 1-1 Sensuicho, Tobata, Kitakyushu 804-8550, Japan

b JST, PRESTO, 4-1-8 Honcho Kawaguchi, Saitama 332-0012, Japan

c JST, ACT-C, 4-1-8 Honcho Kawaguchi, Saitama 332-0012, Japan

d Research Center for Advanced Eco-fitting Technology, Kyushu Institute of Technology, Tobata, Kitakyushu 804-8550, Japan

*Corresponding author

Tel and fax: 81-93-884-3318

E-mail: tohno@che.kyutech.ac.jp

m^2 g^{-1}, has become a bottleneck for further enhancement of photocatalytic activity.

Many methods for improving the specific surface area of g-C$_3$N$_4$ have therefore been proposed. These methods include the twice heating method,[6] exfoliation g-C$_3$N$_4$ by ultrasonic treatment method,[7] and nanocasting with a hard template method.[8]

Among the various methods, morphology control is considered to be an effective means for increasing specific surface area and photocatalytic activity. There have been a few reports on fabrication of g-C$_3$N$_4$-like nanofibers, nanobelts, nanorods, nanotubes and nanowires;[9, 10] however, the XRD pattern of g-C$_3$N$_4$ was changed by morphology control: low-angle reflection peak at 13.1° disappeared.

In this study, we developed a facile method for synthesizing g-C$_3$N$_4$ with a high specific surface area, which has nanotube morphology, by two-step condensation of melamine. In the first step, melamine was hydrothermally treated in water, and as-condensed melamine was heated by a high temperature in the second step. The two-step condensation process controls morphology to increase the specific surface area and the photocatalytic activity of g-C$_3$N$_4$. The enhanced activity of g-C$_3$N$_4$ was evaluated by photodegradation of Rhodamine B (Rh B).

Characterization of melamine and HM-x

Figure 1(a) shows XRD patterns of original melamine and hydrothermally treated melamine. With the hydrothermal reaction, the appearance of new peaks and disappearance of old peaks are assertive evidence for the creation of a new arrangement. A very well-developed lamellar stacking peak,[11] (002), is observed at around 29° after hydrothermal reaction, supporting the observed sheet-like structure. Original melamine and hydrothermally treated melamine were also confirmed by FT-IR spectroscopy. As shown in Figure 1(b), with the hydrothermal treatment, some new peaks appeared in the 1750~1850 cm^{-1} region in both HM-12 and HM-24 that were attributed to C=O stretching vibration,[12] which means that polymerization was carried out and cyanuric acid was formed. It can be expected that the solution will be changed to an alkaline solution by hydrothermal treatment because of the ammonia generated from melamine condensation. Therefore, hydrothermal treatment with an alkaline solution made the melamine portion change into cyanuric acid.[13, 14]
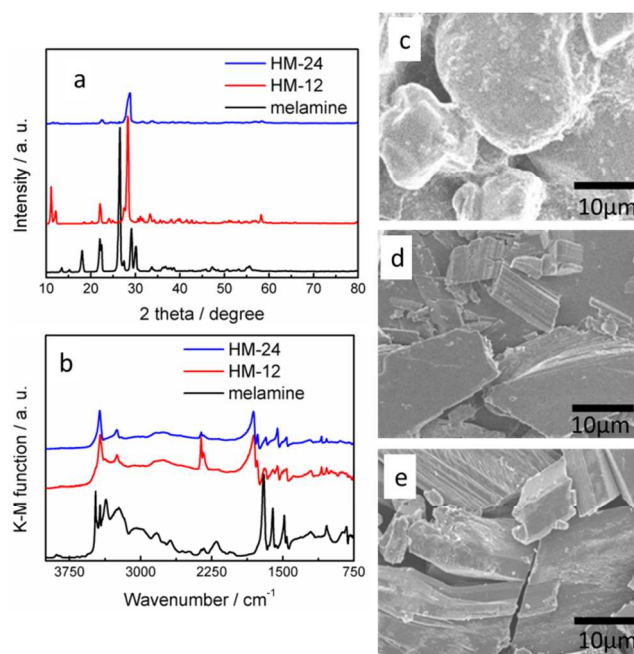
Figure 1 (a) XRD patterns and (b) FT-IR spectroscopy of melamine and hydrothermally treated melamine. SEM images of (c) melamine, (d) HM-12 and (e) HM-24.

Figure 1 (c), (d) and (e) show SEM images of original melamine and the melamine processed at 200℃ in water for 12 hour and 24 hour, respectively. Figure 1(c) shows that the morphology of original melamine is granular with a particle size of 10-50 μm. When the hydrothermal treatment time was increased to 12 hours, the morphology of products became sheet-like (Figure 1(d)), being composed of melamine-cyanuric acid. When the treatment time was increased to 24 hours, the morphology of the products was still a sheet-like structure, and the size of particles became large.

Characterization of Hx-C$_3$N$_4$

Figure 2(a) shows XRD patterns of g-C$_3$N$_4$ obtained after heat treatment. All of the samples gave two peaks consistent with bulk g-C$_3$N$_4$, suggesting that the samples basically have the same crystal structure as that of g-C$_3$N$_4$ (JCPDS 87-1526). The low-angle reflection peak is presumably related to an in-plane structural packing motif at 13.1° (indexed as (100)) of bulk g-C$_3$N$_4$. The low-angle reflection peaks of H12-C$_3$N$_4$ and H24-C$_3$N$_4$ were shifted to 12.9° and 12.8°, respectively. It was confirmed that, compared with bulk g-C$_3$N$_4$, H12-C$_3$N$_4$ and H24-C$_3$N$_4$ have chains that adopt a "zigzag-type" geometry to increase the distance of neighboring tri-s-triazine units.[15] The low-angle reflection peak also becomes less pronounced. This is mainly caused by the simultaneously decreased planar size of the layers during two-step condensation. With respect to bulk g-C$_3$N$_4$, the strong inter-planar stacking peak of aromatic systems around 27.6° (indexed as (002)) is shifted to a higher degree (27.8° and 27.7°, respectively), indicating a decreased gallery distance between the basic sheets in g-C$_3$N$_4$.[16] The (002) peak also becomes broader and gradually less intense with increase the time of hydrothermal treatment, indicating disturbance of the graphitic structure by two-step condensation.

Functional groups of bulk g-C$_3$N$_4$, H12-C$_3$N$_4$ and H24-C$_3$N$_4$ were confirmed by FT-IR spectroscopy. As shown in Figure 2(b), the characteristic IR spectrum of Hx-C$_3$N$_4$ was similar to that of bulk g-
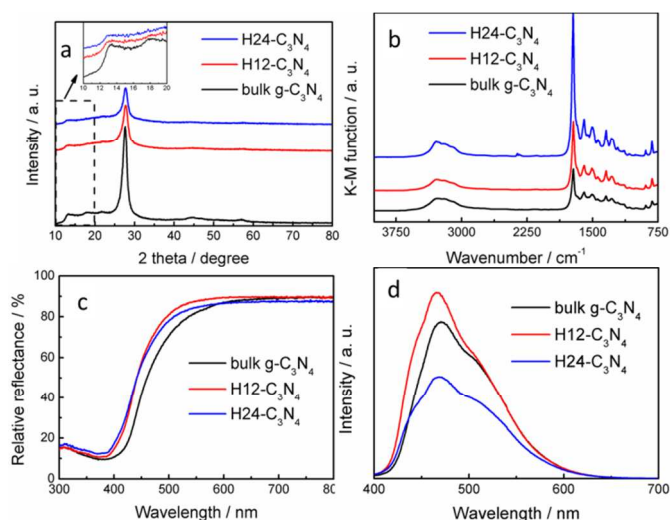

Figure 2 (a) XRD, (b) FT-IR, (c) UV-vis DRS and (d) photoluminescence spectroscopy of the samples obtained by two-step condensation.

C$_3$N$_4$. A peak at about 810 cm^{-1} originating from the heptazine ring system and peaks in the region from 900 to 1800 cm^{-1} attributed to either trigonal C-N(-C)-C or bridging C-NH-C units were observed in all samples.[17, 18] These peaks obviously become sharper, probably due to more ordered packing of bands. The peaks in the 1750~1850 cm^{-1} region disappeared after the second step of condensation, indicating that a more "zigzag-type" geometry arrangement formation may be due to the appearance and disappearance of acid anhydride bonds. Elemental analysis revealed a C/N molar ratio of 0.66 and less than 2 wt% of hydrogen for bulk g-C$_3$N$_4$, and this ratio was almost unchanged with increase the temperature of hydrothermal treatment (Table. 1).

Figure 2(c) shows UV-vis diffuse reflectance spectra (DRS) of the samples. As shown in Figure 2(c), compared with the spectrum of bulk g-C$_3$N$_4$, the spectrum of Hx-C$_3$N$_4$ was blue shifted, probably due to the well-known quantum confinement effect. These results are presumably attributed to decrease in particle size. Actually, the S$_{BET}$ of g-C$_3$N$_4$ was enlarged by two step condensation that H12-C$_3$N$_4$ and H24-C$_3$N$_4$ showed almost 3 times and 5 times higher specific surface areas than that of bulk g-C$_3$N$_4$ (Table 1), respectively.

Figure 2(d) shows photoluminescence spectra of the samples. The excitation wavelength of the photoluminescence spectra is set at 365 nm. With increase in hydrothermal treatment time, a blue shift of the peak wavelength was observed in the fluorescence emission spectra, in accordance with the results of UV-vis DRS. Since photoluminescence properties would be influenced by defects that

Table 1 BET specific surface area and elemental analysis of obtained samples.

	specific surface area (m2 / g)	C (wt%)	H (wt%)	N (wt%)	C/N (mol/mol)
bulk g-C$_3$N$_4$	15	34.71	1.89	61.47	0.659
H12-C$_3$N$_4$	43.6	34.16	1.8	60.49	0.659
H24-C$_3$N$_4$	71.7	34.33	1.77	60.71	0.660

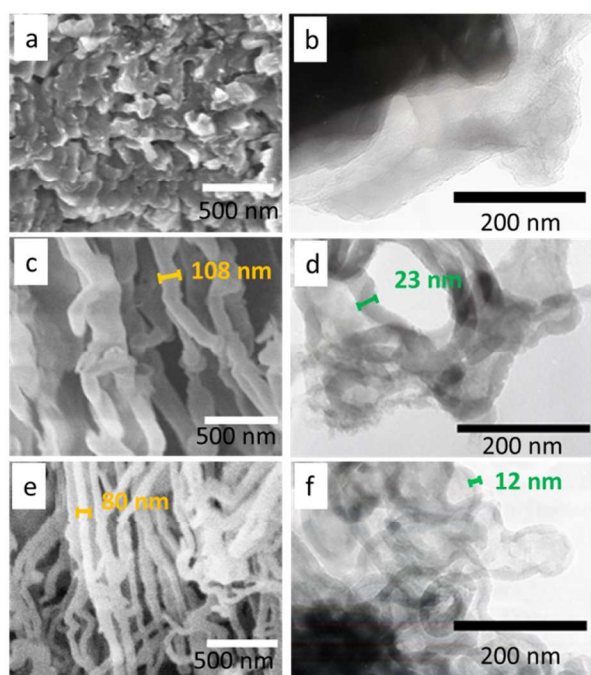**Figure 3** SEM images of (a) bulk g-C_3N_4, (c) H12-C_3N_4 and (e) H24-C_3N_4. TEM images of (b) bulk g-C_3N_4, (d) H12-C_3N_4 and (f) H24-C_3N_4.

can reduce the strength of fluorescence peaks, photoluminescence spectra were also used to determine the number of defects.[19] In Figure 2(d), it can be seen that the number of defects decreased with hydrothermal treatment for 12 hours. After that the number of defects increased when the first-step reaction was up to 24 hours. The increased number of defects is attributed to the appearance and disappearance of more cyanuric acid via the two-step condensation process in H24-C_3N_4.

A scanning electron microscope (SEM) and a transmission electron microscopy (TEM) were used to investigate the textural structure and morphology as shown in Figure 3 (a), (c), (e) and Figure 3 (b), (d), (f), respectively. Bulk g-C_3N_4 showed a sheet-like morphology as expected, but with two-step condensation, H12-C_3N_4 and H24-C_3N_4 both showed nanotube morphology. The diameter of nanotube decreased from around 108 nm to 80 nm over time with hydrothermal treatment. What`s more the wall thickness of the H12-C_3N_4 and H24-C_3N_4 nanotube also decreased from 23 nm to 12 nm. These results were attributed to the appearance and disappearance of cyanuric acid via the two-step condensation process can control the morphology of g-C_3N_4. Therefore, the improved specific surface area was probably due to the change in sheet-like morphology to nanotube structure and decreased sheet thickness of g-C_3N_4 (Table 1).

Photocatalytic activity for photodegradation of Rh B

The photocatalytic activities of the prepared samples were evaluated by photodegradation of Rh B. Details of the photocatalytic measurement and the UV-vis spectroscopic changes of Rh B over catalysts are shown in supporting information (Figure S1). Figure 4 (a) shows photocatalytic activities of the samples (c is the remained concentration of Rh B, and c_0 is the initial concentration of Rh B). As a comparison, without photocatalyst or without light irradiation was carried out, and almost none of Rh B was photodegradation at
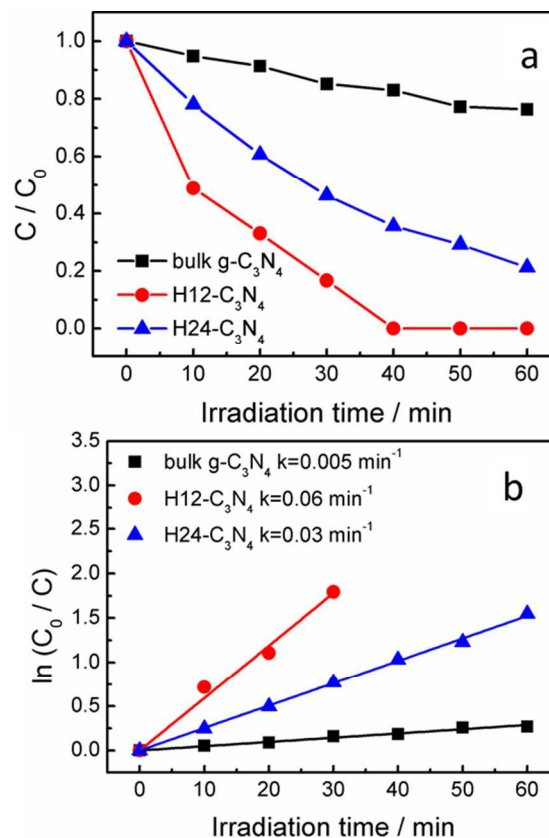

Figure 4 (a) Photocatalytic activities for Rh B photodegradation over bulk g-C_3N_4 and Hx-C_3N_4 samples prepared by two-step condensation. (b) Relationship between Rh B degradation efficiency and the light irradiation time for the bulk g-C_3N_4 and Hx-C_3N_4 photocatalysis system.

all. Bulk g-C_3N_4 shows poor activity, since only 24 % of the Rh B was degraded when the irradiation time lasted for 60 min. On the other hand, the photocatalytic activity of H24-C_3N_4 was much higher than that of bulk g-C_3N_4. Furthermore H12-C_3N_4 shows the highest photocatalytic activity, the Rh B was completely degraded when the irradiation time lasted for 40 min. Figure 4 (b) presented the linear relationship between $\ln(C_0/C)$ and the irradiation time for Rh B degradation. Rate constant k gives an indication of the activity of the photocatalyst. The Rh B photodegradation rate constants for bulk- g-C_3N_4, H12-C_3N_4 and H24-C_3N_4 displayed as 0.005 min⁻¹, 0.06 min⁻¹ and 0.03 min⁻¹, respectively. Although H12-C_3N_4 has a much lower specific surface area than that of H24-C_3N_4, it showed the highest photocatalytic activity, being almost 12 times higher than that of bulk g-C_3N_4. Then the photocatalytic activity decreased with increase in hydrothermal treatment time up to 24 hours. Interestingly, H24-C_3N_4 has an almost 10 times higher specific surface area than that of bulk g-C_3N_4 and 2 times than that of H12-C_3N_4, but its photocatalytic activity was 5 times higher than that of bulk g-C_3N_4 and lower than that of H12-C_3N_4. It can be attributed to two aspects: (i) the blue shift in the light absorption region resulted in reduction of visible light into the reaction system and (ii) as mentioned above, since the defects can act as recombination centers for photogenerated electron-holes,[20] the increase in the number of defects lowered the photocatalytic performance.

To evaluate the stability of nanotube g-C_3N_4, the sample of H12-C_3N_4 was chosen to perform cyclic test. The results are shown in Figure S2. There was no decrease observed in repeating the reaction

three times under the same condition, indicating the good stability of the catalyst during the photocatalytic reaction. In addition, the same results can be seen by XRD analyses (Figure S3).

Conclusions

In this study, nanotube g-C_3N_4 was fabricated from melamine by a simple two-step condensation process. The specific surface area was enlarged by morphology control, and the photocatalytic activity for decomposition of Rh B under visible light irradiation was enhanced. H12-C_3N_4 shows the highest photocatalytic activity which was almost 12 times higher than bulk g-C_3N_4. Since H24-C_3N_4 contained more defects than H12-C_3N_4, result in lower photocatalytic activity than H12-C_3N_4, but still 5 times higher than bulk g-C_3N_4. The results reported may provide a good reference for developing more superior photocatalyst g-C_3N_4 and also provides a new sight to enhance photocatalytic activity of g-C_3N_4 without using template for morphology control and increase specific surface area.

Acknowledgements

Notes and references

1. A. FUJISHIMA AND K. HONDA, *NATURE*, 1972, **238**, 37-38.

2. X. C. WANG, K. MAEDA, A. THOMAS, K. TAKANABE, G. XIN, J. M. CARLSSON, K. DOMEN AND M. ANTONIETTI, *NAT. MATER.*, 2009, **8**, 76-80.

3. Z. JIN, N. MURAKAMI, T. TSUBOTA AND T. OHNO, *APPLIED CATALYSIS B: ENVIRONMENTAL*, 2014, **150–151**, 479-485.

4. S. C. YAN, S. B. LV, Z. S. LI AND Z. G. ZOU, *DALTON TRANS.*, 2010, **39**, 1488-1491.

5. K. KONDO, N. MURAKAMI, C. YE, T. TSUBOTA AND T. OHNO, *APPL. CATAL. B-ENVIRON.*, 2013, **142**, 362-367.

6. P. NIU, L. L. ZHANG, G. LIU AND H. M. CHENG, *ADV. FUNCT. MATER.*, 2012, **22**, 4763-4770.

7. S. YANG, Y. GONG, J. ZHANG, L. ZHAN, L. MA, Z. FANG, R. VAJTAI, X. WANG AND P. M. AJAYAN, *ADVANCED MATERIALS*, 2013, **25**, 2452-2456.

8. A. THOMAS, A. FISCHER, F. GOETTMANN, M. ANTONIETTI, J.-O. MULLER, R. SCHLOGL AND J. M. CARLSSON, *JOURNAL OF MATERIALS CHEMISTRY*, 2008, **18**, 4893-4908.

9. M. TAHIR, C. CAO, N. MAHMOOD, F. K. BUTT, A. MAHMOOD, F. IDREES, S. HUSSAIN, M. TANVEER, Z. ALI AND I. ASLAM, *ACS APPLIED MATERIALS & INTERFACES*, 2013, **6**, 1258-1265.

10. W. B.-N. ZHAO PENG, CHEN XIANG-YING AND Q. YI-TAI, *CHEMICAL RESEARCH IN CHINESE UNIVERSITIES*, 2009, **25**, 412-416.

11. M. SHALOM, S. INAL, C. FETTKENHAUER, D. NEHER AND M. ANTONIETTI, *J. AM. CHEM. SOC.*, 2013, **135**, 7118-7121.

12. Y.-S. JUN, E. Z. LEE, X. WANG, W. H. HONG, G. D. STUCKY AND A. THOMAS, *ADVANCED FUNCTIONAL MATERIALS*, 2013, **23**, 3661-3667.

13. E. KROKE, M. SCHWARZ, E. HORATH-BORDON, P. KROLL, B. NOLL AND A. D. NORMAN, *NEW JOURNAL OF CHEMISTRY*, 2002, **26**, 508-512.

14. E. HORVATH-BORDON, E. KROKE, I. SVOBODA, FUE, R. RIEDEL, S. NEERAJ AND A. K. CHEETHAM, *DALTON TRANSACTIONS*, 2004, 3900-3908.

15. T. SANO, S. TSUTSUI, K. KOIKE, T. HIRAKAWA, Y. TERAMOTO, N. NEGISHI AND K. TAKEUCHI, *J. MATER. CHEM. A*, 2013, **1**, 6489-6496.

16. G. DONG, Y. ZHANG, Q. PAN AND J. QIU, *JOURNAL OF PHOTOCHEMISTRY AND PHOTOBIOLOGY C: PHOTOCHEMISTRY REVIEWS*, 2014, **20**, 33-50.

17. S. C. YAN, Z. S. LI AND Z. G. ZOU, *LANGMUIR*, 2009, **25**, 10397-10401.

18. Y. MENG, G. XIN AND D. CHEN, *OPTOELECTRONICS AND ADVANCED MATERIALS-RAPID COMMUNICATIONS*, 2011, **5**, 648-650.

19. Y. ZANG, L. LI, Y. ZUO, H. LIN, G. LI AND X. GUAN, *RSC ADVANCES*, 2013, **3**, 13646-13650.

20. V. K. MAHAJAN, M. MISRA, K. S. RAJA AND S. K. MOHAPATRA, *JOURNAL OF PHYSICS D: APPLIED PHYSICS*, 2008, **41**, 125307.